



اونيورسيتي تيكنيكل مليسيا ملاك

UNIVERSITI TEKNIKAL MALAYSIA MELAKA

**PLASMA ETCHING PROCESS FOR ALUMINUM-COPPER
METALLIZATION BY PHOTORESIST MARGIN IMPROVEMENT
FOR CMOS 0.13- μ m TECHNOLOGY**



WAN FAIZAL MOHAMED HASSAN

اونيورسيتي تيكنيكل مليسيا ملاك

UNIVERSITI TEKNIKAL MALAYSIA MELAKA

DOCTOR OF ENGINEERING

2022



Faculty of Manufacturing Engineering

**PLASMA ETCHING PROCESS FOR ALUMINUM-COPPER
METALLIZATION BY PHOTORESIST MARGIN IMPROVEMENT
FOR CMOS 0.13- μm TECHNOLOGY**

اونيورسيتي تيكنيكل مليسيا ملاك
UNIVERSITI TEKNIKAL MALAYSIA MELAKA

Wan Faizal Mohamed Hassan

Doctor of Engineering

2022

**PLASMA ETCHING PROCESS FOR ALUMINUM-COPPER METALLIZATION
BY PHOTORESIST MARGIN IMPROVEMENT FOR CMOS 0.13- μm
TECHNOLOGY**

WAN FAIZAL MOHAMED HASSAN



UNIVERSITI TEKNIKAL MALAYSIA MELAKA

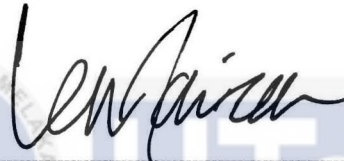
2022

DECLARATION

I declare that this thesis entitled “Plasma Etching Process for Aluminum-Copper Metallization by Photoresist Margin Improvement for CMOS 0.13- μm Technology” is the result of my own research except as cited in the references. The thesis has not been accepted for any degree and is not concurrently submitted in candidature of any other degree.

Signature

:



Name

:

WAN FAIZAL BIN MOHAMED HASSAN

Date

:

7-Mar-2022

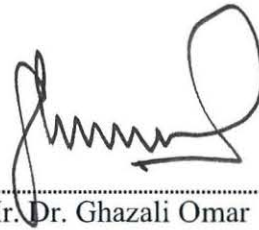


اونيورسيتي تيكنيكل مليسيا ملاك
UNIVERSITI TEKNIKAL MALAYSIA MELAKA

APPROVAL

I hereby declare that I have read this thesis and in my opinion, this thesis is sufficient in terms of scope and quality for the award of Doctor of Engineering.

Signature :



Supervisor Name : Prof. Ir. Dr. Ghazali Omar

PROFESOR IR. TS. DR. GHAZALI BIN OMAR

Timbalan Naib Canselor (Penyelidikan & Inovasi)

Universiti Teknikal Malaysia Melaka

Date :

12/8/2022



UTeM

اونيورسيتي تيكنيكل مليسيا ملاك

UNIVERSITI TEKNIKAL MALAYSIA MELAKA

DEDICATION

To my beloved mother, father and family. All praises to ALLAH and His blessing for the completion of this thesis.



ABSTRACT

In wafer fabrication manufacturing, the aluminum etching process is a dry plasma etching process used as the main process for construction of aluminum copper (AlCu) interconnect structures. As customer requirements changed for faster, more reliable and lower cost chips, chip manufacturers have learned to reduce the size of components on a chip in order to achieve those requirements. As the geometry of the chip is getting smaller, the width of AlCu line wiring specifications is also shrinking. To print the smaller geometry pattern requirements, the photoresist (PR) thickness in the masking process also has to be reduced for better resolution. Such a thinner resist will create a challenge during plasma etching to ensure a minimal resist loss process which will require a new type of equipment. The use of an oxide film as a hard mask has been evaluated by many other researchers. This approach does require a process integration change with full technology qualifications and will easily take many lengthy qualification procedures particularly to qualify the existing products. In SilTerra, the plasma AlCu etching process for 0.13 μ m High Voltage (HV) technology is qualified at the Applied Material (AMAT) DPS+ etcher system. Larger chamber volume design coupled with the use of C₂H₄ patterned passivation gas process is enabling the 0.13 μ m AlCu etching process to run with enough PR margin process. This limited capacity of the AMAT tools triggered SilTerra engineers to initiate process qualification works at the LAM9600PTX chamber which is an equipment designed for 0.16 μ m and bigger technology scale. The initial trial using SilTerra 0.13 μ m technology process failed to meet the process requirements on the PR remaining thickness. The insufficient margin caused deformed AlCu structure formations. This thesis evaluated the use of methane gas during AlCu etching process as an additional passivation gas to the existing nitrogen gas. The AlCu etching rate non-uniformity due to aspect ratio dependent etching (ARDE) is evaluated at a methane gas flow rate within the range of 0 to 18 standard cubic centimeters per minute (SCCM). One factor of a time experiment with comprehensive design of experiment trials is evaluated and it is found that, an addition of methane at 9 SCCM in AlCu etching step able to reduce the ARDE% from 26% to 21% with acceptable incremental of metal width critical dimension. A 60 SCCM of Cl₂ and 10 SCCM of CHF₃ gas mixture has been determined from DOE runs as a replacement gas mixture to the existing Cl₂/O₂ to address organic backside anti-refractive coating (OBARC) etching requirement for lower PR loss process. The true mean value of PR margin thickness and oxide loss margin thickness from the proposed new process conditions have been statistically determined to meet the minimum SilTerra process requirement. The electrical tests on M2B_V and RS_M2C parameters are verified on the production pre-runs and the final sort yield data are validated on the volume runs successfully. This novelty finding is successfully increasing the capacity with an additional 5,000 wafers output per month which is equivalent to USD 2.5 million and a capital expenditure avoidance of USD 5 million.

**PROSES PUNARAN PLASMA UNTUK PELOGAMAN ALUMINIUM-TEMBAGA
OLEH PERBAIKAN MARGIN FOTORINTANG UNTUK TEKNOLOGI CMOS 0.13-
 μm**

ABSTRAK

Dalam pembuatan fabrikasi wafer, proses punaran aluminium-tembaga (AlCu) adalah proses plasma punaran kering yang digunakan sebagai proses utama untuk pembinaan struktur interkoneksi AlCu. Oleh kerana keperluan pelanggan berubah untuk cip yang lebih pantas, dan lebih pelbagai fungsi dengan kos yang lebih rendah, pengeluar cip telah mengurangkan ukuran skala struktur kepada 0.13 μm pada cip untuk mencapai keperluan tersebut. Apabila geometri cip semakin kecil, lebar spesifikasi pendawaian garis AlCu juga menyusut. Untuk mencetak keperluan corak geometri yang lebih kecil, ketebalan fotorintang dalam proses pelindung juga harus dikurangkan untuk resolusi yang lebih baik. Ini akan menimbulkan cabaran semasa pengukuhan plasma untuk memastikan proses kehilangan bahan rintang yang minimum memerlukan peralatan baru. Penggunaan filem oksida sebagai topeng keras telah dinilai oleh penyelidik lain. Pendekatan ini memang memerlukan perubahan integrasi proses dan kelayakan teknologi sepenuhnya dan dengan itu prosedur kelayakan akan lebih panjang terutama untuk memenuhi syarat produk yang sedia ada. Di SilTerra, proses punaran AlCu plasma untuk teknologi 0.13 μm dapat dipenuhi syaratnya dalam sistem Applied Material (AMAT) DPS+. Reka bentuk isipadu ruang yang lebih besar ditambah dengan penggunaan proses gas pasif bercorak C₂H₄ telah memungkinkan proses pengukuhan AlCu 0.13 μm berjalan dengan proses margin fotorintang yang mencukupi. Kapasiti terhadap alat AMAT telah mendorong para jurutera SilTerra untuk memulakan kerja kelayakan proses di peralatan LAM9600PTX yang berkeupayaan untuk skala teknologi 0.16 μm dan lebih besar. Percubaan awal menggunakan proses teknologi SilTerra 0.13 μm gagal memenuhi syarat proses pada ketebalan fotorintang (PR). Margin yang tidak mencukupi telah menyebabkan pembentukan struktur AlCu yang cacat. Tesis ini telah menilai penggunaan gas metana semasa proses punaran AlCu sebagai gas pasifasi tambahan kepada gas nitrogen yang ada. Kadar keseragaman proses punaran AlCu yang tidak seragam kerana kebergantungan kepada nisbah aspek (ARDE) yang dinilai pada kadar aliran gas metana dalam lingkungan 0 SCCM hingga 18 SCCM. Satu faktor eksperimen masa dengan penilaian beberapa percubaan eksperimen reka bentuk yang komprehensif telah didapati bahawa pada 9 SCCM kadar aliran metana telah dapat mengurangkan ARDE% dari 26% hingga 21% dengan terdapat peningkatan pada dimensi kritikal lebar logam. Campuran 60 SCCM Cl₂ dan 10 SCCM CHF₃ telah ditentukan daripada larian DOE sebagai campuran gas pengganti kepada Cl₂/O₂ sedia ada untuk proses punaran lapisan anti-bias belakang organik (OBARC) untuk proses kehilangan PR yang lebih rendah. Nilai min sebenar ketebalan margin PR dan ketebalan margin kehilangan oksida daripada proses punaran baharu yang dicadangkan telah ditentukan secara statistik untuk memenuhi syarat minimum bagi proses punaran logam di SilTerra. Ujian elektrik pada parameter M2B_V dan RS_M2C telah disahkan semasa pra-pengeluaran dan juga data hasil akhir telah disahkan pada pengeluaran tinggi yang berjaya dijalankan. Penemuan baru ini berjaya meningkatkan kapasiti penambahan 5,000 output wafer sebulan yang setara dengan USD 2.5 juta dan mengelakkan dari perbelanjaan modal sebanyak USD 5 juta.

ACKNOWLEDGEMENTS

In the Name of Allah, the Most Gracious, the Most Merciful

First and foremost, I would like to thank and praise Allah the Almighty, my Creator, my Sustainer, for everything I received since the beginning of my life. I would like to extend my appreciation to the SilTerra Malaysia Sdn. Bhd (SMSB) and Universiti Teknikal Malaysia Melaka (UTeM) for providing the research platform. Thank you also to the Malaysian Ministry of Higher Education (MOHE) for the financial assistance.

My utmost appreciation goes to my main supervisor, Profesor Dr. Ghazali Omar, Universiti Teknikal Malaysia Melaka (UTeM) for all his support, advice and inspiration. His constant patience for guiding and providing priceless insights will forever be remembered. Also, to my co-supervisor, Profesor TS. Dr. Noreffendy Bin Tamaldin, Universiti Teknikal Malaysia Melaka (UTeM) who constantly supported my journey. My special thanks go to Dr. Kader Ibrahim and Dr. Mohd Azizi Chik of SMSB for all the help and support I received from them.

Last but not least, from the bottom of my heart a gratitude to my beloved wife, Hasanah Daud, for her encouragements and who has been the pillar of strength in all my endeavors. My eternal love also to my daughter, Wan Nuryazmin, for her patience and understanding. I would also like to thank my beloved parents, Mohamed Hassan and Wan Hasnah for their endless support, love and prayers. Finally, thank you to all the individuals who had provided me the assistance, support and inspiration to embark on my study.

UNIVERSITI TEKNIKAL MALAYSIA MELAKA

TABLE OF CONTENTS

	PAGE
DECLARATION	
APPROVAL	
DEDICATIONS	
ABSTRACT	i
ACKNOWLEDGEMENTS	iii
TABLE OF CONTENTS	iv
LIST OF TABLES	vii
LIST OF FIGURES	xi
LIST OF SYMBOLS AND ABBREVIATIONS	xix
LIST OF APPENDICES	xxii
LIST OF PUBLICATIONS	xxiii
CHAPTER	
1. INTRODUCTION	1
1.1 Background	1
1.2 Problem Statement	3
1.3 Research Objective	7
1.4 Scope of Research	8
1.5 Contribution of Research	9
1.6 Thesis Outline	10
2. LITERATURE REVIEW	12
2.1 Introduction	12
2.2 Manufacturing and IC fabrication overview	14
2.3 Review of plasma etching past and present	19
2.4 Review for business outlook for More-than-Moore products	27
2.5 Aluminum-Copper (AlCu) alloy interconnect	29
2.6 Metallization etching theory	31
2.6.1 TiN etching	39
2.6.2 AlCu etching	40
2.7 Bottom anti-reflection coating (BARC)	44
2.8 Metal etching process qualification	48
2.9 Etch processing equipment	51
2.10 Application of parametric test for metal etch process in validation	55

2.11	Review of experimental methodology approach	58
2.12	Summary	59
3.	MATERIALS AND ETHODOLOGY	63
3.1	Introduction	63
3.2	Equipment and material for the methodology	72
3.3	Methodology flow	85
3.4	Equipment and test wafers preparations	88
	3.4.1 Installation of methane gas	88
	3.4.2 Test wafers preparation	90
3.5	Experiment of new metal etching process	92
3.6	Developing new OBARC etching step	95
	3.6.1 The effect of Cl ₂ and CHF ₃ on photoresist removal rate evaluated on blanket PR wafer	96
	3.6.2 The effect of Cl ₂ and CHF ₃ in OBARC/TiN etching step on Metal-2 pattern wafers	97
	3.6.3 Verification of photoresist remaining thickness on Metal-2 pattern wafer at higher Cl ₂ flow rate in OBARC etching step	102
3.7	Final profile validation for physical characteristic	104
3.8	Product validation on electrical and sort	106
3.9	Summary	110
4.	RESULT AND DISCUSSION	112
4.1	Introduction	112
4.2	The effect of methane flow on photoresist etch rate (PRER)	113
4.3	Phase 1 - results of varying methane flow on etching characteristic – ARDE, photoresist remaining thickness and metal width dimension	115
4.4	Phase 2 - optimization of BARC etching step	128
	4.4.1 The effect of Cl ₂ and CHF ₃ on photoresist etch rate (evaluated on a blanket PR wafer)	129
	4.4.2 The effect of Cl ₂ and CHF ₃ in BARC and TiN etching step on residue defect in the etching area	139
	4.4.3 The effect of Cl ₂ and CHF ₃ in BARC and TiN etching step on metal width dimension	143
4.5	XSEM validation of Metal-2 photoresist remaining thickness profile at higher flow of Cl ₂ , 60 and 70 SCCM (extrapolated condition)	147
4.6	Phase 3 - final validation on physical characteristics of Metal-2 patterns after etching – benchmarking to Metal-2 process I/O requirement	148
	4.6.1 Verification of true mean value of photoresist remaining thickness for new process conditions	149
	4.6.2 Verification of true mean value on oxide loss/recess for new process conditions	154
	4.6.3 Verification of Cl ₂ flow margin in BARC and TiN etching steps against residue defect in etching area	158
	4.6.4 Verification of sidewall quality against CH ₄ flow variation in AlCu etching (ME) step	159
	4.6.5 Corrosion test performance	161

4.7	Phase 4 - product validation on electrical and sort – benchmarking to customer specifications	164
4.7.1	First level product verification (split lots) – sort yield data	164
4.7.2	First level product verification (split lots) – M2B_V data	172
4.7.3	First level product verification (split lots) – RS_M2C data	181
4.7.4	Second level product verification (volume run) – FICD trend	190
4.7.5	Second level product verification (volume run) – sort yield data	194
4.8	Summary	195
4.9	Economic impact analysis	198
5.	CONCLUSION AND RECOMMENDATIONS	199
5.1	Conclusion	199
5.2	Future works	202
	REFERENCES	204
	APPENDICES	232



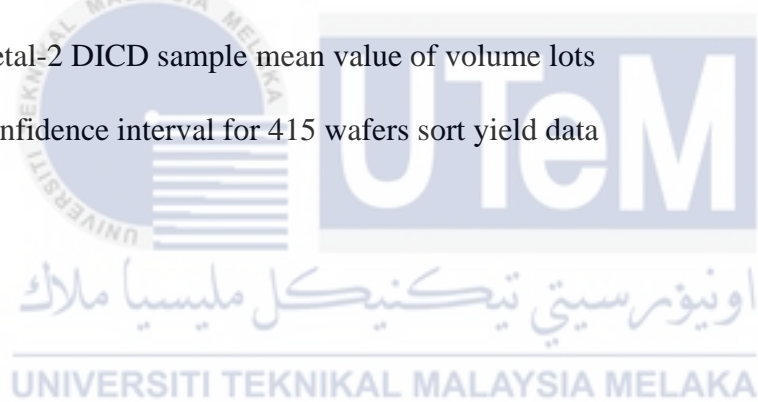
LIST OF TABLES

TABLE	TITLE	PAGE
1.1	Summary of LAM9600PTX metal etch chemistry by steps in SilTerra for 0.16 μ m technology	6
2.1	Bond energies and enthalpies of free radicals formation	21
2.2	SilTerra metal etch physical characteristics requirements	51
2.3	Equipment comparison between LAM9600PTX and AMAP DPS+ metal etch equipment in SilTerra	52
2.4	Summary of previous experimental methodology in various plasma etching processes	59
2.5	Comparison of previous work in resolving erosion of photoresist during plasma etching	61
3.1	List of equipment used	73
3.2	Data input during chamber idling for SilTerra LAM9600PTX metal etcher	75
3.3	Detail of process parameters for M4K_NC13 recipe	75
3.4	Example of data input requirement to measure critical dimensions at KLA8100XP	77
3.5	Example of the FICD measurement data output	79
3.6	Example of data output from Agilent HP4072A	81
3.7	Example of film thickness measurement data points from Optiprobe 3290. Flm thickness value is reported in unit of Angstrom and tabulated in the column “Thickness Value”	83

3.8	Process recipe to evaluate the effect of varying methane on PRER	88
3.9	ME partial process recipe template for microloading study on methane flow rate variable in main etch (ME) step	93
3.10	Methane gas flow rate variables in main etch (ME) step for each experimental run	94
3.11	Tabulation of data extraction from XSEM analysis for ARDE calculation	95
3.12	Experimental plan of Cl ₂ and CHF ₃ flow rates on the photoresist removal rate (PRER)	97
3.13	Recipe content for OBARC etching step	97
3.14	Experimental plan using metal-2 pattern wafer	98
3.15	Example of tabulation result for defect counts and FICD measurement from each experimental run	99
3.16	Physical characterization acceptance criteria for Metal-2 of C13HV technology node	105
3.17	Electrical characterization acceptance criteria for Metal-2 of C13HV technology node	109
3.18	Checklist for experiment and its status	111
4.1	Parameter of step 7 conditions of 4 runs to determine AlCu ARDE percentage at different flow of methane	116
4.2	Summary of raw data measured from SEM images for parameter a, b, c, d and calculated ARDE %	119
4.3	ANOVA of the model with P-value 0.0003	123

4.4	Quantiles and Shapiro-Wilk test on PRER raw data with non-normal distribution (Experiment no. 3, Table 3.18)	131
4.5	Results of PRER for each experimental runs at alpha of 0.05 for sample mean confidence interval	134
4.6	Defect inspection counts and FICD results for each experimental run	139
4.7	Photoresist thickness profile XSEM result for 60 SCCM and 70 SCCM Cl ₂ in BARC step verified against SilTerra outgoing requirements	148
4.8	Final metal etch recipe conditions	149
4.9	Summary of photoresist remaining thickness obtained from XSEM analysis for 6 samples etched with new metal etching condition	150
4.10	Quantile and Shapiro-Wilk test on photoresist remaining thickness with normal distribution (Experiment no. 6, Table 3.18)	152
4.11	Confidence interval of photoresist remaining thickness (new process conditions)	153
4.12	Confidence interval of photoresist remaining thickness at wafer center (new process conditions)	154
4.13	Confidence interval of photoresist remaining thickness at wafer edge (new process conditions)	154
4.14	Summary of oxide loss obtained from XSEM analysis for 6 Samples etched with new metal etching conditions as detailed in Table 4.7	155
4.15	Quantile and Shapiro-Wilk test on oxide recess/loss thickness with normal distribution (Experiment no. 6, Table 3.18)	156
4.16	Confidence interval of oxide loss thickness (new process conditions)	157

4.17	Confidence interval of oxide loss thickness at wafer center (new process conditions)	158
4.18	Confidence interval of oxide loss thickness at wafer edge (new process conditions)	158
4.19	Split lot sort yield confidence Interval for new conditions etched at Metal-2	169
4.20	Split lot sort yield confidence interval for benchmarked conditions (Standard) etched at Metal-2	171
4.21	Metal-2 FICD sample mean value of new process	190
4.22	Metal-2 DICD sample mean value of volume lots	192
4.23	Confidence interval for 415 wafers sort yield data	195



LIST OF FIGURES

FIGURE	TITLE	PAGE
1.1	AlCu alloy interconnect metallization in an integrated circuit	2
1.2	Metal-2 XSEM profile with insufficient PR remaining thickness	5
2.1	Illustration of IC fabrication stages	15
2.2	Re-entrant process flow in semiconductor wafer fabrication line	16
2.3	Druvesteyn electron energy distribution of a cold plasma	21
2.4	Ion-assisted gas surface chemistry using Ar ⁺ and XeF ₂ on silicon	22
2.5	Plasma etching sidewall profiles	24
2.6	Illustration of dense metal pattern structure partially etched until main etch step	26
2.7	SilTerra technology portfolio	28
2.8	AlCu alloy interconnect metallization consists of multilayer films	32
2.9	Metal stack film in VLSI/ULSI integration	33
2.10	Metal stack profile in VLSI/ULSI after metal etching process and photoresist stripping process	34
2.11	Illustration of schematic diagram for LAM9600PTX metal etcher system	35
2.12	Multi-step plasma metal etching process sequence in LAM9600 PTX chamber	38
2.13	An illustration of cross section view of a portion of integrated circuit to illustrate the BARC layer underlying on substrate	45
2.14	BARC etching rate of different types with different combinations of etching chemistries	47

2.15	Snapshot of SilTerra process flow plan in Metal-2 etch module indicating processing step names	50
2.16	Illustration of metal etch cross section indicating common metal etch problems	51
2.17	Schematic drawing of high density plasma etching system with inductively coupled plasma (ICP) Source	53
2.18	Parametric test performed after wafer fabrication completed and before functional product verification	55
2.19	Comb-serpentine structure	56
2.20	Test pad arrangement showing location of comb-serpentine test structure in between Pad 15 and Pad 16 for SilTerra C13HV technology	56
2.21	Relationship of resistance (R) and sheet resistance (ρ_s) of serpentine metal structure	57
3.1	Flowchart for the methodology experiment	64
3.2	Illustration of typical configuration of LAM9600PTX equipment and associated stripper modules	74
3.3	200mm wafer layout indicating the 5 field measurement point locations	77
3.4	Layout of 49-Site Polar Map at 3 mm Edge Exclusion	82
3.5	Example of SEM image of isolated metal line structure	84
3.6	Example of SEM image of dense metal line structures	84
3.7	Installation of CH ₄ gas cylinder to LAM9600PTX chamber	86
3.8	Process flowchart to verify the effect of methane on PRER	87
3.9	Schematic of methane gas line connected to LAM9600PTX chamber gas box via a CH ₄ mass flow controller (MFC)	89

3.10	Example of EDC system that records and stores the scheduled equipment monitoring index such as PRER for each equipment in SilTerra	90
3.11	SilTerra blanket photoresist test wafer preparation workflow	91
3.12	SilTerra metal-2 short loop wafer preparation workflow	92
3.13	Example of partial profile XSEM result from sample etched until main etch step	95
3.14	Process workflow of Metal-2 pattern wafer preparation and etching process plan for sidewall inspection	101
3.15	SilTerra workflow to determine metal etch photoresist remaining thickness and oxide loss/recess	103
3.16	Example of metal profile cross sectional analysis in dense structures to determine photoresist remaining (a) and oxide loss/recess (b)	104
4.1	The effect of methane flow on photoresist etch rate (PRER)	114
4.2	SEM image cross section for run 1	117
4.3	SEM image cross section for run 2	117
4.4	SEM image cross section for run 3	118
4.5	SEM image cross section for run 4	118
4.6	Illustration of open area etching and small feature etching due to aspect ratio dependant etching (ARDE) effect	120
4.7	Microloading in ARDE% of AlCu etching as a function of methane flow rate in main etch (ME) step	123
4.8	The effect of methane flow on photoresist (PR) remaining (primary axis) and metal line width (secondary axis)	125
4.9	Effect of methane flow on AlCu endpoint time etching	125

4.10	Metal line width versus methane flow rate	126
4.11	Normal quantile plot of photoresist etch rate (PRER) raw data (Experiment no. 3, Table 3.18)	130
4.12	Contour plot for the etch rate from run#1	131
4.13	Box plot on PRER in each experimental run with 49 measurement points per wafer and histogram shows all runs with dual data distribution	131
4.14	Confidence interval of PRER from run#1 is within 1191-1240 at 95% confidence level	133
4.15	Fit model analysis with constructed model effect of Cl_2 , CHF_3 and Cl_2*CHF_3	135
4.16	The leverage plot for Cl_2 factor shows confidence curve (red line) - crosses horizontal line	136
4.17	The leverage plot for CHF_3 factor shows confidence curve (red line) – does not cross horizontal line	136
4.18	PRER stdev by Cl_2 flow rate	138
4.19	Final regression plot of PRER and Cl_2 with P-value of 0.0008	138
4.20	SEM images for Run 7 at MPDense (a) center, (b) edge	140
4.21	SEM images for Run7 at MPISO (a) center, (b) edge	140
4.22	Fit model for residue defect count response	141
4.23	Prediction profiler of Cl_2 and CHF_3 against defect count response	142
4.24	Interaction profiles of Cl_2 and CHF_3 flow rate on residue defect counts observed in etching area	143
4.25	Fit model for FICD	145
4.26	Prediction profiler of Cl_2 and CHF_3 term on FICD	146

4.27	Interaction profile of Cl ₂ and CHF ₃ term on FICD	147
4.28	Sample 3 of XSEM image to determine photoresist thickness and oxide loss/recess cut from center location of wafer	150
4.29	Normal quantile plot of photoresist remaining thickness data etched with new process condition (Experiment no. 6, Table 3.18)	152
4.30	Oneway analysis of photoresist thickness by sample location at wafer center and edge	153
4.31	Normal quantile plot of oxide recess/loss thickness data etched with new process condition (Experiment no. 6, Table 3.18)	156
4.32	Oneway analysis of oxide loss/recess by sample locations at wafer center and edge	157
4.33	SEM inspection images for residue defect verification in open etching area at 50, 60 and 70 SCCM of Cl ₂ in the BARC and TiN etching step	159
4.34	SEM image of dense metal lines for sidewall verification on wafer sample run at 5 SCCM of CH ₄ in ME Step	160
4.35	SEM image of dense metal lines for sidewall verification on wafer sample run at 15 SCCM of CH ₄ in ME Step	161
4.36	KLA-Tencor defect maps scanned on wafer sample ID S8P10252 of 0hr, 24hr wetbox, 48hr drybox, 72hr drybox for corrosion performance verification	163
4.37	KLA-Tencor defect count of wafer sample ID S8P10252 at each scan hour shows no increment in defect counts after 24hr wetbox and 72hrs drybox Test	164

4.38	1st level product validation on three split lots – Standard conditions (39 wafers) and NEW conditions (34 wafers)	166
4.39	Normal quantile plot for split lot sort yield data distribution (34 wafers) etched with new conditions at Metal-2	168
4.40	Normal quantile plot for split lot sort yield data distribution (39 wafers) etched with benchmarked conditions (Standard)	170
4.41	T-test of mean sort yield between Metal-2 New (34 wafers) and Metal-2 STD (39 wafers) conditions	172
4.42	Normal quantile plot of M2B_V Data for NEW conditions (KQQ37126.1) with normal distribution, Shapiro-Wilk test P-value of 0.8515	173
4.43	Normal quantile plot of M2B_V data for standard (STD) conditions (KQQ37126.1) with normal distribution, Shapiro-Wilk test P-value of 0.5671	174
4.44	T-test for M2B_V data based on KQQ37126.1 split lot	175
4.45	Normal quantile plot of M2B_V data for NEW conditions (KQQ37049.1) with normal distribution, Shapiro-Wilk test P-value of 0.6145	176
4.46	Normal quantile plot of M2B_V data for standard (STD) conditions (KQQ37049.1) with normal distribution, Shapiro-Wilk test P-value of 0.2353	177
4.47	T-test for M2B_V data based on KQQ37049.1 split lot	178

4.48	Normal quantile plot of M2B_V data for NEW conditions (KQQ37036.1) with normal distribution, Shapiro-Wilk test P-value of 0.4341	179
4.49	Normal quantile plot of M2B_V data for standard (STD) conditions (KQQ37036.1) with normal distribution, Shapiro-Wilk test P-value of 0.3518	180
4.50	T-test for M2B_V data based on KQQ37036.1 split lot	181
4.51	Normal quantile plot of RS_M2C data for NEW conditions (all 3 split lots in Figure 4.38) with non-normal distribution, Shapiro-Wilk test P-value of 0.0006	182
4.52	Normal quantile plot of RS_M2C data for standard (STD) conditions (all 3 split lots in Figure 4.38) with non-normal distribution, Shapiro-Wilk test P-value of <0.0001	183
4.53	X by Y analysis for NEW and STD conditions based on split lots	184
4.54	Variability chart for RS_M2C by lot within split condition	185
4.55	Correlation of RS_M2C and FICD for new conditions with $r = -0.8628$	187
4.56	Correlation of RS_M2C and FICD for standard (STD) conditions with $r = -0.9294$	188
4.57	Variability chart for FICD by lot sample mean within split condition	189
4.58	Metal-2 FICD trend chart of new process from volume lots against spec limit	191
4.59	Capability analysis of Metal-2 FICD etched with new onditions having Cpk of 1.487	192
4.60	Metal-2 DICD trend chart of volume lots against spec limit	193

4.61 Sort yield data for 415 wafers etched with final conditions in
LAM9600PTX

195

